The Size and Shape of Caldesmon and Its Fragments in Solution Studied by Dynamic Light Scattering and Hydrodynamic Model Calculations

Edward A. Czuryło,* Thomas Hellweg,# Wolfgang Eimer,# and Renata Dąbrowska*
*Department of Muscle Biochemistry, Nencki Institute of Experimental Biology, Warsaw, Poland, and #Department of Chemistry, Physical Chemistry 1, University of Bielefeld, Bielefeld, Germany

ABSTRACT The size and the shape of caldesmon as well as its 50-kDa central and 19-kDa C-terminal fragments were investigated by photon correlation spectroscopy. The hydrodynamic radii, which have been calculated from the experimentally obtained translational diffusion coefficients, are 9.8 nm, 6.0 nm, and 2.9 nm, respectively. Moreover, the experimental values for the translational diffusion coefficients are compared with results obtained from hydrodynamic model calculations. Detailed models for the structure of caldesmon in solution are derived. The contour length is about 64 nm for all of the models used for caldesmon.

INTRODUCTION

Caldesmon is a major actin-binding protein found in smooth muscle and nonmuscle cells (for a review, see Marston and Redwood, 1991; Walsh, 1991; Sobue and Sellers, 1991; Dąbrowska, 1994; Marston and Huber, 1996). Smooth-muscle caldesmon is a multifunctional protein that binds tightly and specifically to protein components of the contractile apparatus (actin, myosin, and tropomyosin) (Sobue et al., 1981; Smith et al., 1987; Ikebe and Reardon, 1988). Its inhibitory effect on the tropomyosin-potentiated, actin-activated Mg^{2+}-ATPase activity of myosin is regulated by a Ca^{2+}-calmodulin complex (Sobue et al., 1982; Dąbrowska et al., 1985; Chalovich et al., 1987; Marston and Redwood, 1992). Another regulatory mechanism is the phosphorylation of caldesmon by casein kinase II (Sutherland et al., 1994) or by protein kinase C (Vorotnikov et al., 1994). These observations prompted the speculation that caldesmon may be involved in auxiliary mechanisms for regulation of the smooth-muscle contraction (Chalovich, 1988; Marston, 1989; Brenner et al., 1991).

Two cDNA clones have been sequenced for chicken gizzard caldesmon. One represents a 756-amino acid residue isoform (Bryan et al., 1989), and the other a 771-residue isoform (Hayashi et al., 1989) with molecular masses of 87 kDa and 89 kDa, respectively. The larger isoform corresponds to a 15-residue peptide insertion into the central region of the smaller isoform. Both isoforms are present in chicken gizzard muscle (Riseman et al., 1989), and for convenience we will refer to the amino acid sequence of the smaller isoform.

Secondary structure studies of chicken gizzard caldesmon revealed that it is a highly helical protein. The estimation from caldesmon CD spectra gave 40–51% helicity (Czuryło et al., 1993; Graceffa and Jancsó, 1993). Predictions from the amino acid sequence showed that the central region of the molecule contains a 175-residue (Czuryło et al., 1993) or 165-residue helix with a length of about 38 nm (Wang et al., 1991a). Moreover, an extended structure was postulated for the whole molecule (Czuryło et al., 1993). This postulate was in good agreement with observations of caldesmon on electron micrographs (Mabuchi and Wang, 1991) and with sedimentation experiments (Graceffa et al., 1988; Malencik et al., 1989; Stafford et al., 1994).

From the results described above, one may postulate that smooth-muscle caldesmon contains three functionally distinct regions. The N-terminal region binds to myosin (Katayama et al., 1989; Velaz et al., 1990), whereas the C-terminal region binds to actin, Ca^{2+}-calmodulin, and tropomyosin and inhibits actomyosin ATPase activity (Szpacenko and Dąbrowska, 1986; Chalovich et al., 1987, 1992; Fujii et al., 1987; Wang et al., 1991b). The 27-nm-long, rodlike, helical central region acts as a spacer between N-terminal and C-terminal regions and is missing in the nonmuscle isoform of caldesmon (Sobue and Sellers, 1991).

The aim of this work was to investigate the hydrodynamic properties of smooth-muscle caldesmon and its fragments and, based on the experimental results from dynamic light scattering (DLS), to model the caldesmon molecule. DLS provides a measurement of the structure of biological material in solution (native state), without strong perturbation of the sample.

MATERIALS AND METHODS

Preparation of caldesmon and its fragments

Caldesmon was prepared from chicken gizzard muscle according to the procedure described by Bretscher (1984). Its purification procedure is described by Czuryło et al. (1991). The 19-kDa and 50-kDa fragments were obtained by chemical cleavage of caldesmon at cysteines (Riseman et al., 1989; Nefsky and Bretscher, 1989). After the cleavage reaction was

Received for publication 30 July 1996 and in final form 13 November 1996.

Address reprint requests to Prof. Renata Dąbrowska, Department of Muscle Biochemistry, Nencki Institute of Experimental Biology, 3 Pasteur Street, 02-093 Warsaw, Poland. Tel.: 4822-222802; Fax: 4822-225342; E-mail: renata@nencki.gov.pl.

Dr. Hellweg's present address is CRPP, Av. du Docteur Schweitzer, 33600 Pessac, France.

0006-3495/97/02/835/08 $2.00

terminated by the addition of dithiothreitol (DTT), the reaction mixture was dialyzed against a buffer containing 25 mM imidazole/HCl (pH 7.0), 50 mM NaCl, 1 mM EGTA, and 1 mM NaN_3 (buffer A). The respective fragments were purified by liquid chromatography on a DEAE-Sepharose Fast Flow column (45 × 3 cm), which was equilibrated with buffer A. Elution was performed with a linear NaCl gradient (50–300 mM). The collected flow-through fraction containing the nonretarded 19-kDa fragment, and the fractions containing the 50-kDa fragment eluted with NaCl gradient in buffer A, were pooled, lyophilized, and dialyzed against 25 mM Tris/HCl (pH 7.5), 50 mM NaCl, 1 mM EGTA, and 1 mM NaN_3 (buffer B). Thereafter, both fractions were rechromatographed on a CM-Sepharose Fast Flow column (45 × 2.5 cm), with buffer B as the solvent, and eluted with the NaCl gradient as before. The final purification of each fragment was achieved by molecular sieve chromatography in a Bio-Gel A-0.5 m column (125 × 1.5 cm) (Czuryło et al., 1991).

The digestion reaction and the homogeneity of the protein fragments were monitored by sodium dodecyl sulfate-polyacrylamide gel electrophoresis according to the method of Laemmli (1970). To obtain samples usable for light scattering experiments, the proteins were dialyzed against a 20 mM imidazole buffer (pH 7.0) containing 100 mM NaCl, 1 mM EGTA, 1 mM DTT, and 1 mM NaN_3 (buffer C), refreshing the dialysate every 2 h over a period of 10–14 h, unless otherwise mentioned. Afterward, each solution was clarified by centrifugation for 2 h at 140,000 × g. The concentration of the caldesmon and its fragments was determined by UV absorption using the following absorption coefficients for 0.1% solutions at a wavelength of 279 nm: chicken gizzard caldesmon, 0.400 (Czuryło et al., 1993); 19-kDa C-terminal fragment, 1.130 (Czuryło et al., 1993); and 50-kDa fragment, 0.252 (calculated using molar absorption coefficients of tyrosine and tryptophan 1405 and 5579 $M^{-1}\,cm^{-1}$, respectively; Mihaly, 1968).

Photon correlation spectroscopy

The normalized electrical field autocorrelation function $g^1(\tau)$ of the scattered electrical field E_S contains information about the translational motion of the protein.

$$g^1(\tau) = \langle E_s^*(t)E_s(t+\tau)\rangle/\langle I\rangle. \quad (1)$$

E_S^* is the complex conjugate of E_S, and I is the scattered intensity.

This function can be obtained directly in a so-called heterodyne experiment. Much easier to perform is the homodyne experiment, which yields $g^2(\tau)$:

$$g^2(\tau) = \langle E_s^*(t)E_s(t)E_s^*(t+\tau)E_s(t+\tau)\rangle/\langle I\rangle^2. \quad (2)$$

These two functions are related through the Siegert relation:

$$g^2(\tau) = 1 + C|g^1(\tau)|^2, \quad (3)$$

where C is the coherence factor and depends on the experimental conditions. For a monodisperse dilute solution, $g^1(\tau)$ is represented by a single exponential,

$$g^1(\tau) = \exp(-\Gamma\tau), \quad (4)$$

with $\Gamma = Dq^2$, where D is the translational diffusion coefficient, and $q = [(4\pi n)/\lambda]\sin(Q/2)$, the length of the scattering vector.

In reality, for most samples one must deal with a distribution of relaxation rates due to polydispersity or contributions from high-molecular-weight impurities, and the decay of the correlation function must be described by a weighted sum of exponentials:

$$g^1(\tau) = \int_0^\infty G(\Gamma)\exp(-\Gamma\tau)d\Gamma. \quad (5)$$

Here $G(\Gamma)$ is the distribution function of relaxation rates (Berne and Pecora, 1976). The correlation functions were analyzed by the method of cumulants (Koppel, 1972) and by an inverse Laplace transformation of Eq. 5, using the FORTRAN program CONTIN (Provencher, 1982a,b). These methods provide a weight-averaged apparent translational diffusion coefficient for the scattering particles:

$$D = kT/(6\pi\eta R_s). \quad (6)$$

Herein k is the Boltzmann constant, η is the solvent viscosity, and R_S is the Stokes radius.

Using CONTIN is preferable for samples with low scattering intensities, where minor contributions of dust particles may seriously affect the correlation function. Some larger, slowly moving particles, which may be present in the samples as impurities, will also contribute to the correlation function. CONTIN offers the possibility of discriminating these contributions to the long time tail of the correlation function from the relevant relaxation modes.

The concentration dependence of the experimentally obtained translational diffusion coefficient (D_{exp}) is described by

$$D_{exp} = D^0(1 + k_D c), \quad (7)$$

where D^0 is the self-diffusion coefficient; k_D ($= 2A_2M_w - k_f - \nu$) is the dynamic virial coefficient, which contains information about thermodynamic (through the second osmotic virial coefficient A_2) and frictional (through k_f) effects; and ν is the the partial specific volume of the protein.

In addition to the size of the diffusing molecules (given by the Stokes radius), it is possible to obtain information about the shape of the molecule from the ratio of the frictional coefficients f/f_{theo}. The frictional coefficients f and f_{theo} are defined by the Stokes equation,

$$f = 6\pi\eta R_s. \quad (8)$$

Thus the ratio of the frictional coefficients is equivalent to the ratio of the respective radii:

$$f/f_{theo} = R_s/(R_s)_{theo}. \quad (9)$$

The theoretical hydrodynamic radius, $(R_s)_{theo}$, is obtained from

$$(R_s)_{theo} = [(3M\nu)/(4\pi N_A)]^{1/3}. \quad (10)$$

Here N_A is the Avogadro constant, ν is the partial specific volume, and M is the molar mass of the investigated protein (Eimer et al., 1993). $(R_s)_{theo}$ is the radius a protein of mass M would have were it a sphere. Therefore, if the ratio f/f_{theo} is equal to unity, the molecule adopts a spherical shape in solution. Higher values indicate anisotropic structures.

Sample preparation for the DLS measurements

The protein solutions have been filtered into dust-free sample cells through filters with a pore size of 0.1 μm (Anotop, Whatman). Thereafter, the samples were centrifuged for 0.5 h at approximately 1000 × g. This is necessary to remove larger dust particles and air bubbles. The DLS experiments were carried out at (283.1 ± 0.1) K. All of the experimental results discussed in the following are mean values from three different measurements. The experiments have been reproduced with two different preparations of the protein. A detailed description of the DLS setup can be found elsewhere (Patkowski et al., 1990b). An argon ion laser operated in single mode at a wavelength of λ_0 = 488 nm with a typical output power of 400 mW was used as the light source. The sample cell (rectangular fluorescence cell with a path length of 10 mm) was immersed in a toluene bath for refractive index matching. Data were collected on an ALV-5000 multi-tau correlator at different scattering angles. The data analysis, using CONTIN and the method of cummulants, was performed on a HP workstation.

Hydrodynamic model calculations

In dilute solutions of noninteracting particles the diffusion coefficient is related to the hydrodynamic radius by the Stokes-Einstein equation (Eq. 6). If one calculates the radius by the use of Eq. 6, the obtained value is the radius of a sphere that is hydrodynamically equivalent to the scattering particle. This apparent radius also contains information about the anisotropy of the macromolecules. This is due to the fact that anisotropic particles cannot be described with a simple scalar diffusion coefficient. Instead, their diffusional behavior must be described by a translational diffusion tensor Ξ, and the measured value for D is given by the following expression:

$$D = [\mathrm{Trace}(\Xi)]/3. \quad (11)$$

The structures of rigid polymers such as proteins can be approximated by simple models built from spherical subunits (beads). With these bead models it is possible to perform hydrodynamic calculations, which yield the translational diffusion coefficient D of the model structure (Garcia Bernal and Garcia de la Torre, 1981). This value can be compared to experimental results obtained by DLS.

In the formalism of these calculations the beads are regarded as frictional centers. They can be characterized by a 3×3 frictional tensor. The influence of one bead subunit on the other subunits of the model is expressed in terms of hydrodynamic interaction tensors. In the calculations presented here we used the original Oseen tensor, which regards the beads as point sources of friction, and two modified tensors (Garcia de la Torre and Bloomfield, 1977), which are valid for nonidentical and nonoverlapping and identical overlapping beads (Rotne and Prager, 1969). If the model for a macromolecule consists of identical overlapping beads, the calculations are performed using the Rotne-Prager tensor, which has been modified by Garcia de la Torre and Bloomfield (1981) to incorporate the possibility of calculations with models containing nonoverlapping beads of nonidentical radius. The use of the modified tensor for models containing overlapping beads results in a slight overestimation of the friction exhibited by the model structure and therefore in a slight underestimation of the values for the diffusion coefficient.

The differences in the values calculated using the Rotne-Prager tensor and the Oseen tensor are small for models with very elongated structures (Riseman and Kirkwood, 1950). The translation-rotation coupling is taken into account in these calculations by the inversion of a 6×6 resistance matrix (Garcia Bernal and Garcia de la Torre, 1980). One can use this method of modeling to get an idea of the structure of a protein in solution, when the hydrodynamic properties of the protein are known from experiments (Eimer et al., 1993).

RESULTS

We have investigated the two fragments and the intact caldesmon molecule by DLS. The obtained correlation functions have been analyzed using CONTIN and, in the case of monomodal functions, by applying the method of cumulants. In the following we refer only to the CONTIN results, but for monomodal correlation functions the results obtained with the method of cumulants are identical within experimental error (data not shown).

C-terminal 19-kDa fragment of caldesmon

The C-terminal 19-kDa fragment of caldesmon consists of 177 amino acid residues from Cys^{580} to the terminal amino acid residue, which is Pro^{756}. In contrast to the 50-kDa fragment, and intact caldesmon DLS measurements of the C-terminal 19-kDa fragment were performed in 30 mM phosphate buffer (pH 5), containing 100 mM NaCl, 1 mM EGTA, 1 mM DTT, and 1 mM NaN_3, because in buffer C this fragment revealed a tendency to form high-molecular-weight aggregates. The concentration dependence of the translational diffusion coefficient of the 19-kDa fragment is shown in Fig. 1. An increase in the diffusion coefficient with decreasing concentration was still observable, and a linear extrapolation to zero concentration gave $D^0_{283.1K} = (5.45 \pm 0.27) \times 10^{-7}$ cm^2/s. According to Eq. 6 we calculated $D^0_{293.1K} = (7.0 \pm 0.27) \times 10^{-7}$ cm^2/s, which led to an estimation of the Stokes radius of $R_s = 2.9$ nm. Assuming a value of 0.73 cm^3/g for the partial specific volume of the protein (Eimer et al., 1993), we calculated (according to Eq. 9) the frictional ratio f/f_o. A value of 1.7 obtained for the 19-kDa fragment indicates its slightly anisotropic structure in solution.

Central 50-kDa fragment of caldesmon

According to the prediction of the secondary structure (Marston and Redwood, 1991; Wang et al., 1991a; Czuryło et al., 1993), the central 50-kDa fragment of caldesmon should consist of two helical regions containing 175 and 75 amino acid residues, respectively. Based on previous observations (Wang et al., 1991a), a rodlike structure is expected for this fragment.

The DLS measurements of the 50-kDa fragment were performed in buffer C. The sample revealed no tendency to aggregate, and Fig. 1 clearly indicates a lack of any significant concentration dependence of the experimentally deter-

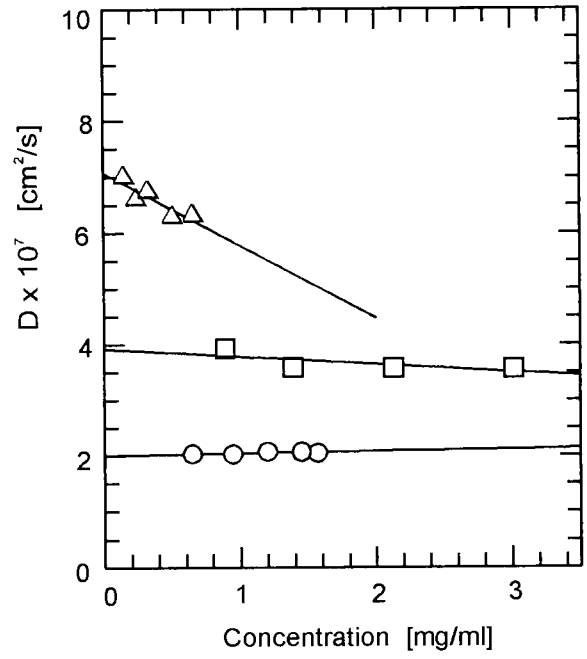

FIGURE 1 Concentration dependence of normalized diffusion coefficients of the caldesmon and its fragments. Diffusion coefficients were normalized to 293.15 K. ○, Caldesmon; □, 50-kDa fragment; and △, 19-kDa fragment of caldesmon.

mined translational diffusion coefficient. In this case it is straightforward to extract the self-diffusion coefficient D^0 from the mean value of all measurements, giving $D^0_{293.1K} = (3.7 \pm 0.2) \times 10^{-7}$ cm^2/s, which yields a hydrodynamic radius of 6 nm. The resultant larger frictional ratio of 2.5, as compared to that of the 19-kDa fragment, implies a more elongated structure of the central fragment of caldesmon in solution than that of the 19-kDa fragment.

Intact caldesmon

The DLS measurements of the whole caldesmon molecule were performed at 283.1 K in buffer C. Similarly, as in the case of the 50-kDa fragment, the translational diffusion coefficient of the intact protein did not depend on the concentration (Fig. 1). The value obtained for the translational diffusion coefficient was $D^0_{293.1K} = (2.1 \pm 0.2) \times 10^{-7}$ cm^2/s and gave a Stokes radius of 9.8 nm. The frictional ratio for the intact caldesmon molecule was calculated to be $f/f_o = 3.4$, suggesting a rodlike structure for the protein molecule. Because of the pronounced elongated structure of the molecule it was necessary to study the angular dependence of the translational diffusion coefficient, to make sure that the investigated relaxation process is purely diffusive and that internal dynamics of the molecule did not significantly contribute to the correlation function. As shown in Fig. 2, the average relaxation rate is dependent on the scattering vector, as expected from Eq. 4.

Table 1 gives an overview of the experimental results. The hydrodynamic radii of the fragments and intact caldesmon increases with molecular weight. However, very different frictional ratios obtained suggest that the 50-kDa fragment and the intact protein exhibit a distinct anisotropic molecular shape.

Hydrodynamic modeling

To generate bead models of the 50-kDa fragment and the intact caldesmon molecule for hydrodynamic calculations,

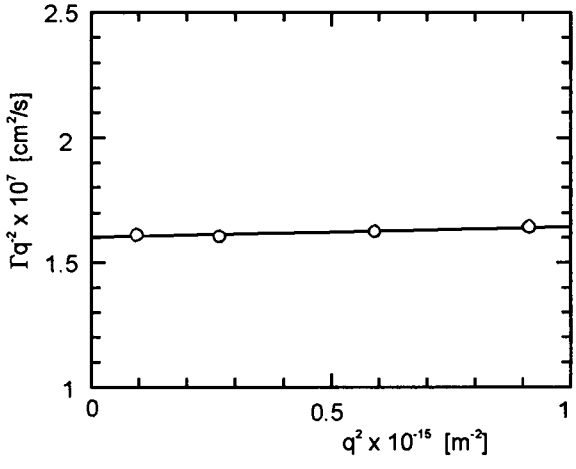

FIGURE 2 Angular dependence of translational diffusion coefficient of caldesmon. Caldesmon concentration was about 1.5 mg/ml.

TABLE 1 Hydrodynamic properties of caldesmon and its fragments

	Intact caldesmon	50-kDa fragment	19-kDa fragment
$D^0_{293.1K} \times 10^7$ (s/cm^2)	2.1	3.7	7.0
R_s (nm)	9.8	6.0	2.9
f/f_0	3.4	2.5	1.7

we took into account information obtained from electron micrographs (Mabuchi and Wang, 1991) and CD spectra (Wang et al., 1991a; Czuryło et al., 1993).

First of all, the experimentally determined translational diffusion coefficients for the 19-kDa as well as the 50-kDa fragments and the intact caldesmon molecule are significantly higher than expected for a spherical molecule of the same molecular weight, already indicating that the individual particles exhibit an anisotropic structure in solution. Second, the native protein reveals the highest frictional ratio, which suggests that the two fragments are organized in the caldesmon molecule in such a way that the overall shape of the protein becomes more elongated (anisotropic).

DLS results, in agreeement with sedimentation data (Wang et al., 1991a), confirmed helical structure predictions of the 50-kDa fragment. Accordingly, the simplest assumption about the shape of the 50-kDa fragment is a rodlike structure, approximated by a linear array of overlapping beads.

Model A in Fig. 3 comprises 85 overlapping beads with a radius of 0.5 nm (Wang et al., 1991a). The total length of the model is 43 nm. The translational diffusion coefficient was calculated to give $D_{293.1K} = 4.44 \times 10^{-7}$ cm^2/s, using the Rotne-Prager tensor for overlapping beads (Garcia de la Torre and Bloomfield, 1977; Rotne and Prager, 1969). For model B we increased the bead radius to 1 nm, which corresponds to the typical diameter for an α-helix. In this structural model with 97 beads, the total length increases to 50 nm. Using the Rotne-Prager tensor we obtained a translational diffusion coefficient of $D_{293.1K} = 3.92 \times 10^{-7}$ cm^2/s for model B. To confirm that the 50-kDa fragment does not form dimers due to dipole-dipole interactions, we also calculated the translational diffusion coefficient of the dimeric structure (Fig. 3, model C), in which each rod has a length of 50 nm. The diffusion coefficient accordingly decreased to $D_{293.1K} = 3.18 \times 10^{-7}$ cm^2/s. In addition, we computed the translational diffusion coefficient for a kinked model structure consisting of two linear parts, which enclose an angle of 135°. The lengths of the two arms were chosen to be 15.5 nm and 39 nm, respectively. We used this model because other experimental data (Marston and Redwood, 1991; Czuryło et al., 1993) indicate that the molecule may have a flexible, globular part in the position of the kink in our model D in Fig. 3. For the diffusion coefficient we obtained $D_{293.1K} = 3.37 \times 10^{-7}$ cm^2/s. We also considered a kinked dimer, but the calculated diffusion coefficient was much too small to be consistent with the experimental data. Hence, for the 50-kDa fragment we could rule out the

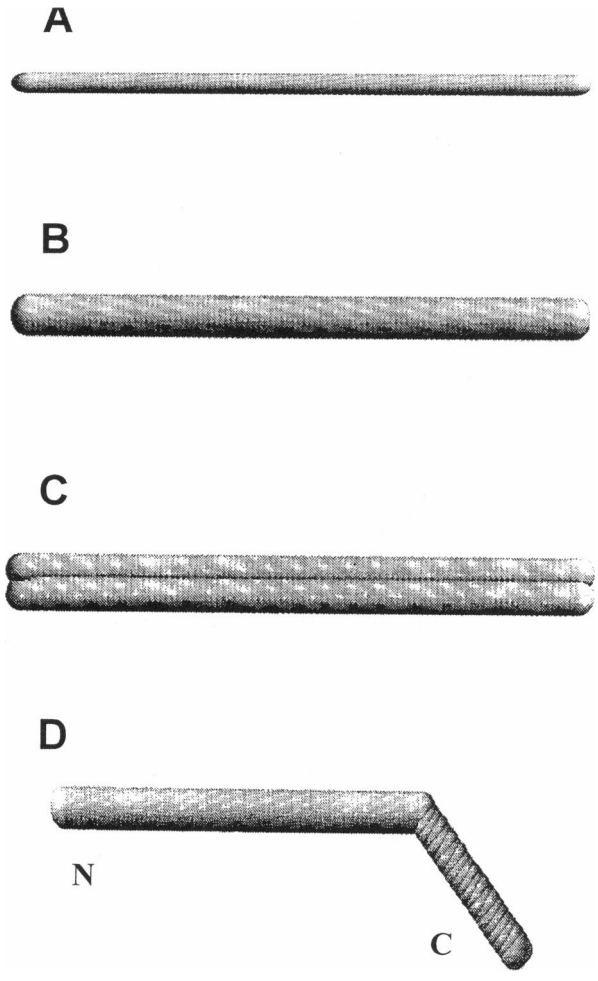

FIGURE 3 Models of the 50-kDa fragment of caldesmon. In model *A* the fragment has a length of 43 nm and a diameter of 1 nm, in model *B* it has the same length but a diameter of 2 nm, in model *C* it is a dimer (with a diameter of 2 nm for each monomer), and in model *D* it has a kinked structure with an angle of 135°.

existence of dimers under the given experimental conditions. Model B and model D in Fig. 3 are in good agreement with the experimental value of $D^0_{293.1K} = 3.7 \times 10^{-7}$ cm^2/s. An overview of the calculated values is given in Table 2. The data computed on the basis of the original Oseen tensor are shown only for the purpose of comparison, because the use of this tensor can produce deviations in the case of the models used, because of the fact that the beads are only regarded as point sources of friction in this description of hydrodynamic interaction.

TABLE 2 Diffusion coefficients for four models of the 50-kDa fragment of caldesmon calculated with two different tensors

Model*	Oseen tensor $D_{293.1K} \times 10^7$ (cm^2/s)	Rotne-Prager tensor $D_{293.1K} \times 10^7$ (cm^2/s)
A	—	4.44
B	3.81	3.92
C	3.15	3.18
D	3.45	3.37

*See models in Fig. 3.

The correspondence of translational diffusion coefficient values calculated for the 50-kDa fragment models (taking into account its 2-nm diameter) with the experimental value obtained for this fragment indicates that either the helix is unhydrated or its diameter under hydrated status is smaller than generally accepted. The central segment of caldesmon is rich in Glu and Lys residues. Peptides containing these amino acid residues are strong helix formers, probably because of the generation of intrahelical salt bridges (especially when Glu and Lys occupy i and $i + 4$ positions) (Marqusee and Baldwin, 1987). In the 50-kDa fragment of caldesmon, about 60 salt bridges may be formed (whereas in the 19-kDa fragment there are only six). These may either decrease the accessibility of water molecules to the helix surface, or increase helix compactness (resulting in a decrease in helix diameter). This problem was widely discussed by Wang et al. (1991a).

The hydrodynamic calculations for the intact caldesmon molecule are based on our results for the 50-kDa fragment. The different model structures are displayed in Fig. 4. Assuming a straight rodlike conformation for the central region of the protein, we simply extended model B at both ends by two beads with a radius of 3 nm to obtain model E. The radius of the end beads was treated as equivalent to the hydrodynamic radius of the C-terminal 19-kDa fragment as obtained from our DLS experiments. The translational diffusion coefficients calculated for this model are $D_{293.1K} = 2.28 \times 10^{-7}$ cm^2/s (modified tensor) and $D_{293.1K} = 2.41 \times 10^{-7}$ cm^2/s (Oseen tensor). These values are already in good agreement with the experimental value of $D_{293.1K} = 2.1 \times 10^{-7}$ cm^2/s. For the other structural models proposed, we used a kinked conformation for the central region, as in the case of model D of the 50-kDa fragment. In these models we varied the size and shape of the kink region and the C-terminal end. The simple kinked model F in Fig. 4 consists of two beads with 3-nm radius (globular ends of the protein) and of two linear arrays of beads with radius 1 nm, which enclose an angle of 135°. The shorter rodlike part has a length of 14 nm and the longer, a length of 38 nm. The contour length is 64 nm. As for model E, the radius of the globular end groups was chosen to be 3 nm, in accordance with the hydrodynamic radius obtained from the experimental data of the 19-kDa fragment (see Table 1).

We tried to make some more sophisticated models by taking into account that the kink region is probably globular (Czuryło et al., 1993). Furthermore, the anisotropic structure of the C-terminal 19-kDa fragment, which we can derive from our experimental results for this part of the protein, was also considered. Model G in Fig. 4 contains a bead with radius 2 nm at the position of the kink, and correspondingly the α-helical parts are modeled by fewer beads. The length of the longer part is 41 nm (including the N-terminus), whereas the shorter part has a length of 23 nm (including the C-terminus). This gives a contour length

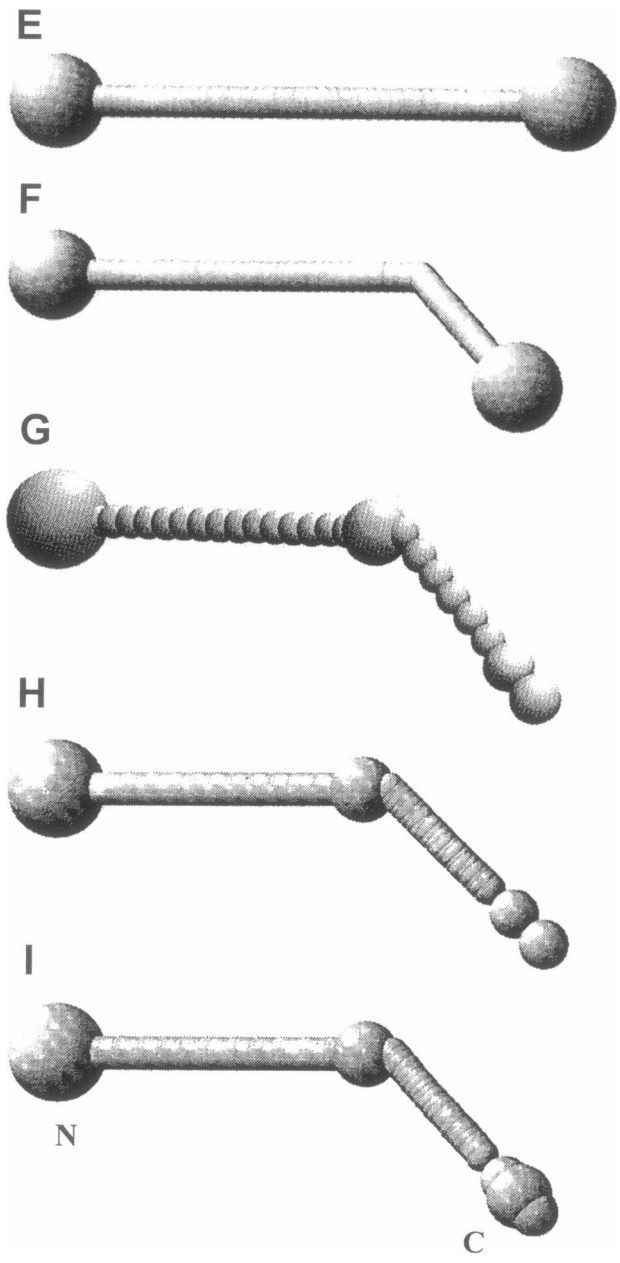

FIGURE 4 Models of intact caldesmon molecule. Model *E* is based on model *B* of the central, 50-kDa fragment (Fig. 3), which is extended with 3-nm-radius beads at both ends, representing N- and C-terminal parts of the molecule. Model *F* is based on model *D* of the 50-kDa fragment (Fig. 3) extended with 3-nm-radius beads at the N- and C-termini, as in model *E*. Models *G*, *H*, and *I* are also based on model *D* of the 50-kDa fragment, but the kink region is supplemented with 2-nm-radius beads, and the size and shape of the 19-kDa fragment vary. In model *G* there are fewer beads in the helical parts than in model *D*; in model *H* the arrangement of beads is the same as in model *G*, but the helical parts consist of twice the number of beads; and in model *I* the 19-kDa fragment is represented by three successive beads with radii of 1.5, 2.0, and 1.5 nm arranged in an ellipsoid. The contour length of all models is approximately equal to 64 nm.

again of approximately 64 nm. Model H in Fig. 4 has the same dimensions as model G, but the helical parts consist of twice the number of beads, generating a smoother surface. In model I the C-terminal part of the caldesmon molecule is represented by three overlapping beads with radii of 1.5 nm, 2.0 nm, and, again, 1.5 nm, instead of only two beads of radius 1.5 nm, to account for the slightly anisotropic shape of this end region as indicated by the frictional ratio (see light scattering results).

Table 3 clearly indicates that the calculated transport properties for the various models are not very different, and all of them agree with the experimental value of the translational diffusion coefficient of the intact caldesmon molecule.

DISCUSSION

To get a more detailed insight into the molecular structure of caldesmon in solution, we combined information from DLS experiments on two different fragments and the intact protein with detailed hydrodynamic model calculations. The experimental results show that the caldesmon molecule exhibits a strongly anisotropic structure in solution. If one compares the diffusion coefficients of caldesmon with the translational diffusion coefficients of less elongated proteins of similar molecular mass, the difference is obvious. For example, for gelsolin (84 kDa) a translational diffusion coefficient of $D^0_{293.1\ K} = 5.5 \times 10^{-7}$ cm^2/s has been obtained (Patkowski et al., 1990b). This value is more than two times higher than the translational diffusion coefficient determined for caldesmon (2.1×10^{-7} cm^2/s). The same applies to the 50-kDa fragment of caldesmon. The translational diffusion coefficient measured for this part of caldesmon (3.7×10^{-7} cm^2/s) is much lower than for G-actin (7.9×10^{-7} cm^2/s; 42 kDa; Patkowski et al., 1990a) or the C-terminal part of gelsolin (7.0×10^{-7} cm^2/s; 43 kDa; Hellweg et al., 1993).

To further elucidate of the anisotropic structure of caldesmon in solution, we performed hydrodynamic model calculations using bead model formalism. Having investigated independently the 50-kDa fragment, it was possible to start hydrodynamic modeling of intact caldesmon from its middle part, for which a long helical structure was assumed. Model calculations for this part of caldesmon using a simple rod, kinked rod, and dimer of rods, approximated by arrays of overlapping beads, were performed. Taking into account the experimental error and the error of the model calculations among the models considered (see Fig. 3), only simple and kinked rod models (B and D) could be viewed as a

TABLE 3 Translational diffusion coefficients calculated for five different models of caldesmon

Model*	modified tensor $D_{293.1K}$ $\times 10^7$ (cm^2/s)	Oseen tensor $D_{293.1K}$ $\times 10^7$ (cm^2/s)
E	2.28	2.41
F	2.15	2.28
G	2.37	2.32
H	1.97	2.44
I	1.97	2.45

*See models in Fig. 4.

plausible representation of the 50-kDa fragment. The contour length and the diameters of the models B and D for the 50-kDa fragment of caldesmon are in good agreement with caldesmon observations on electron microscopy images (Mabuchi and Wang, 1991; Mabuchi et al., 1993).

Models B and D of the 50-kDa fragment were used as a starting point for the construction of models for the intact caldesmon molecule. Completion of these models with spheres or ellipsoids representing N- and C-terminal parts allowed us to generate models of the whole caldesmon molecule (see Fig. 4). The values for the translational diffusion coefficient that have been computed using these model structures (models H, I, and F) are close to each other and close to the experimental translational diffusion coefficient, which suggests that the computable transport properties of highly elongated molecules are not very sensitive to the anisotropy of smaller parts, but are sensitive mainly to their overall length. The contour length of the model structures for caldesmon was kept constant, at approximately 64 nm. This length of the model structures clarifies the observations of electron microscopic images of caldesmon complexes with monoclonal antibodies specific for the N-terminal 28-kDa region of the molecule and for the C-terminal 10-kDa part of caldesmon (Mabuchi et al., 1993), where distances in this range have been found. This is also in accordance with observations of micrographs of caldesmon cross-linked with calmodulin (Mabuchi and Wang, 1991) and biotinylated caldesmon (Katayama and Ikebe, 1995).

Recently Graceffa (1995), who applied cross-linking and fluorescence methods, confirmed earlier observations indicating that the C-terminus of caldesmon is able to bind filamentous actin, whereas the N-terminus is not. A lack of contact between the actin filaments and the N-terminal part of caldesmon has been observed, irrespective of the presence of tropomyosin. These findings suggest that the tertiary structure of the caldesmon molecule on the thin filament is compatible with the structural models we have derived for caldesmon in solution.

Within the experimental error and the assumptions made for the calculations, all models for caldesmon yield translational diffusion coefficients that are in agreement with the experimentally determined value. The models in Fig. 4 can be seen as boundary structures for the caldesmon molecule in solution. From these results one may conclude that the caldesmon molecule contains two rigid segments and exerts some flexibility related to the domain between two helical regions (domain 5), as was suggested before (Czuryło et al., 1993). At the ends of the different models for caldesmon, we located globular or slightly ellipsoidal structures (built up by two or three beads). These structures could represent the molten globules seen on micrographs as flexible, 20-nm-long segments at the ends of the caldesmon molecule (Mabuchi and Wang, 1991). This idea of molten globules is consistent with previous observations (Graceffa and Jancsó, 1993; Czuryło et al., 1993). The loose structures of molten globules become compact when interaction takes place. This has been observed on micrographs of caldesmon cross-linked with calmodulin (Mabuchi and Wang, 1991), and caldesmon complexes with antibodies (Mabuchi et al., 1993) or with avidin (Katayama and Ikebe, 1995).

The contour length in the structural models for caldesmon was 64 nm in all bead models. This is about 10 nm shorter than the value suggested earlier for chicken gizzard caldesmon (Graceffa et al., 1988), but 12 nm longer than suggested for turkey gizzard caldesmon (Malencik et al., 1989). The presented kinked models for caldesmon (see models F–I) may lead to a clearer understanding of the whisker-like projections seen on reconstituted and native thin filaments observed on micrographs of rotary shadowed (Mabuchi et al., 1993) or on negatively stained (Katayama and Ikebe, 1995; Vibert et al., 1993) preparations. These models may also clarify the 35–38 nm periodicity on negatively stained images of arrays formed from chicken gizzard thin filaments precipitated with antibodies specific to the N-terminus of caldesmon (Moody et al., 1990).

The authors wish to gratefully acknowledge the financial support of the DFG (SFB 223) to the University of Bielefeld and the Polish State Committee for Scientific Research to the Nencki Institute.

REFERENCES

Berne, B. J., and R. Pecora. 1976. Dynamic Light Scattering. John Wiley and Sons, New York.

Brenner, B., L. C. Yu, and J. M. Chalovich. 1991. Parallel inhibition of active force and relaxed fiber stiffness in skeletal muscle by caldesmon: implications for the pathway to force generation. *Proc. Natl. Acad. Sci. USA.* 88:5739–5743.

Bretscher, A. 1984. Smooth muscle caldesmon. Rapid purification and F-actin cross-linking properties. *J. Biol. Chem.* 259:12873–12880.

Bryan, J., M. Imai, R. Lee, P. Moore, R. G. Cook, and W.-G. Lin. 1989. Cloning and expression of smooth muscle caldesmon. *J. Biol. Chem.* 264:13873–13879.

Chalovich, J. M. 1988. Caldesmon and thin-filament regulation of muscle contraction. *Cell Biophys.* 12:73–85.

Chalovich, J. M., J. Bryan, C. E. Benson., and L. Velaz. 1992. Localization and characterization of a 7.3-kDa region of caldesmon which reversibly inhibits actomyosin ATPase activity *J. Biol. Chem.* 267:16644–16650.

Chalovich, J. M., P. Cornelius, and C. E. Benson. 1987. Caldesmon inhibits skeletal actomyosin subfragment-1 ATPase activity and the binding of myosin subfragment-1 to actin. *J. Biol. Chem.* 262:5711–5716.

Czuryło, E. A., V. I. Emelyanenko, E. A. Permyakov, and R. Dąbrowska. 1991. Spectrofluorimetric studies on C-terminal 34-kDa fragment of caldesmon. *Biophys. Chem.* 40:181–188.

Czuryło, E. A., S. Y. Venyaminov, and R. Dąbrowska. 1993. Studies on secondary structure of caldesmon and its C-terminal fragments. *Biochem. J.* 293:363–368.

Dąbrowska, R. 1994. Actin and thin-filament-associated proteins in smooth muscle. *In* Airways Smooth Muscle: Biochemical Control of Contraction and Relaxation. D. Raeburn and M. A. Giembycz, editors. Birkhauser Verlag, Basel. 31–59.

Dąbrowska, R., A. Goch, B. Gałązkiewicz, and H. Osińska. 1985. The influence of caldesmon on ATPase activity of skeletal muscle actomyosin and bundling of actin filaments. *Biochim. Biophys. Acta.* 842: 70–75.

Eimer, W., M. Niermann, M. A. Eppe, and B. M. Jokusch. 1993. Molecular shape of vinculin in aqueous solution. *J. Mol. Biol* 229:146–152.

Fujii, T., M. Imai, G. C. Rosenfeld, and J. Bryan. 1987. Domain mapping of chicken gizzard caldesmon. *J. Biol. Chem.* 262:2757–2763.

Garcia Bernal, J. M., and J. Garcia de la Torre. 1980. Transport properties and hydrodynamic centers of rigid macromolecules with arbitrary shapes. *Biopolymers.* 19:751–766.

Garcia Bernal, J. M., and J. Garcia de la Torre. 1981. Transport properties of oligomeric subunit structures. *Biopolymers.* 20:129–139.

Garcia de la Torre, J., and V. A. Bloomfield. 1977. Hydrodynamic properties of macromolecular complexes. 1. Translation. *Biopolymers.* 16: 1747–1763.

Garcia de la Torre, J., and V. A. Bloomfield. 1981. Hydrodynamic properties of complex, rigid biological macromolecules: theory and application. *Q. Rev. Biophys.* 14:81–139.

Graceffa, P. 1995. Cross-linking and fluorescence study of the COOH- and NH_2-terminal domains of intact caldesmon bound to actin. *J. Biol. Chem.* 270:30187–30193.

Graceffa, P., and A. Jancsó. 1993. Secondary structure and thermal stability of caldesmon and its domains. *Arch. Biochem. Biophys.* 307:21–28.

Graceffa, P., C.-L. A. Wang, and W. F. Stafford. 1988. Caldesmon. Molecular weight and subunit composition by analytical ultracentrifugation *J. Biol. Chem.* 263:14196–14202.

Hayashi, K., K. Kanda, F. Kimizuka, I. Kato, and K. Sobue. 1989. Primary structure and functional expression of h-caldesmon complementary DNA. *Biochem. Biophys. Res. Commun.* 164:503–511.

Hellweg, Th., H. Hinssen, and W. Eimer. 1993. The Ca^{2+}-induced conformational change of gelsolin is located in the carboxyl-terminal half of the molecule. *Biophys. J* 65:799–805.

Ikebe, M., and S. Reardon. 1988. Binding of caldesmon to smooth muscle myosin. *J. Biol. Chem.* 263:3055–3058.

Katayama, E., K. Y. Horiuchi, and S. Chacko. 1989. Characteristics of the myosin and tropomyosin binding regions of the smooth muscle caldesmon. *Biochem. Biophys. Res. Commun.* 160:1316–1322.

Katayama, E., and M. Ikebe. 1995. Mode of caldesmon binding to smooth muscle thin filament: possible projection of the amino-terminal domain of caldesmon from native thin filament. *Biophys. J.* 68:2419–2428.

Koppel, D. E. 1972. Analysis of macromolecular polydispersity in intensity correlation spectroscopy: the method of cumulants. *J. Chem. Phys.* 57:4814–4820.

Laemmli, U. K. 1970. Cleavage of the structural proteins during the assembly of the head of bacteriophage T4. *Nature.* 227:680–685.

Mabuchi, K., J. J.-C. Lin, and C.-L. A. Wang. 1993. Electron microscopic images suggest both ends of caldesmon interact with actin filaments. *J. Muscle Res. Cell Motil.* 14:54–64.

Mabuchi, K., and C.-L. A. Wang. 1991. Electron microscopic studies of chicken gizzard cal-desmon and its complexes with calmodulin. *J. Muscle Res. Cell Motil.* 12:145–151.

Malencik, D. A., J. Ausio, C. E. Byles, B. Modrell, and S. R. Anderson. 1989. Turkey gizzard caldesmon: molecular weight determination and calmodulin binding studies. *Biochemistry.* 28:8227–8233.

Marqusee, S., and R. L. Baldwin. 1987. Helix stabilization by $Glu^{-}\cdots Lys^{+}$ salt bridges in short peptides of de novo design. *Proc. Natl. Acad. Sci. USA.* 84:8898–8902.

Marston, S. B. 1989. What is latch? New ideas about tonic contraction in smooth muscle. *J. Muscle Res. Cell Motil.* 10:97–100.

Marston, S. B., and P. A. A. Huber. 1996. Caldesmon. *In* Biochemistry of Smooth Muscle Contraction. M. Barany, editor. Academic Press, San Diego, CA. 77–90.

Marston, S. B., and C. S. Redwood. 1991. The molecular anatomy of caldesmon. *Biochem. J.* 279:1–16.

Marston, S. B., and C. S. Redwood. 1992. Inhibition of actin-tropomyosin activation of MgATPase activity by the smooth muscle regulatory protein caldesmon. *J. Biol. Chem.* 267:16796–16800.

Mihaly, E. 1968. Numerical values of the absorbances of aromatic amino acids in acid, neutral, and alkaline solutions. *J. Chem. Eng. Data.* 13:179–182.

Moody, C., W. Lehman, and R. Craig. 1990. Caldesmon and the structure of smooth muscle thin filaments: electron microscopy of isolated thin filaments. *J. Muscle Res. Cell Motil.* 11:176–185.

Nefsky, B., and A. Bretscher. 1989. Landmark mapping: a general method for localizing cystein residues within a protein. *Proc. Natl. Acad. Sci. USA.* 86:3549–3553.

Patkowski, A., W. Eimer, G. Schneider, B. M. Jokusch, and Th. Dorfmuller. 1990a. The molecular dimensions of G-actin in solution as studied by dynamic light scattering. *Biopolymers.* 30:1281–1287.

Patkowski, A., J. Seils, H. Hinssen, and Th. Dorfmuller. 1990b. Size, shape parameters, and Ca^{2+}-induced conformational change of the gelsolin molecule: a dynamic light scattering study. *Biopolymers.* 30:427–435.

Provencher, S. W. 1982a. A constrained regularization method for inverting data represented by linear algebraic or integral equations. *Comput. Phys. Commun.* 27:213–217.

Provencher, S. W. 1982b. Contin: a general purpose constrained regularization program for inverting noisy linear algebraic and integral equations. *Comput. Phys. Commun.* 27:229–242.

Riseman, J., and J. G. Kirkwood. 1950. The intrinsic viscosity, translational and rotatory diffusion constants of rod-like macromolecules in solution. *J. Chem. Phys.* 18:512–516.

Riseman, V. M., W. P. Lynch, B. Nefsky, and A. Bretscher. 1989. The calmodulin and F-actin binding sites of smooth muscle caldesmon lie in the carboxyl-terminal domain whereas the molecular weight heterogeneity lies in the middle of the molecule. *J. Biol. Chem.* 264:2869–2875.

Rotne, J., and S. Prager. 1969. Variational treatment of hydrodynamic interaction in polymers. *J. Chem. Phys.* 50:4831–4837.

Smith, C. W. J., K. Pritchard, and S. B. Marston. 1987. The mechanism of Ca^{2+} regulation of vascular smooth muscle thin filaments by caldesmon and calmodulin. *J. Biol. Chem.* 262:116–122.

Sobue, K., K. Morimoto, M. Inui, K. Kanda, and S. Kakiuchi. 1982. Control of actin-myosin interaction of gizzard smooth muscle by calmodulin- and caldesmon-linked flip flop mechanism. *Biomed. Res.* 3:188–196.

Sobue, K., Y. Muramoto, M. Fujita, and S. Kakiuchi. 1981. Purification of a calmodulin- binding protein from chicken gizzard that interacts with F-actin. *Proc. Natl. Acad. Sci. USA.* 78:5652–5655.

Sobue, K., and J. R. Sellers. 1991. Caldesmon, a novel regulatory protein in smooth muscle and nonmuscle actomyosin systems. *J. Biol. Chem.* 266:12115–12118.

Stafford, W. F., J. M. Chalovich, and P. Graceffa. 1994. Turkey gizzard caldesmon molecular weight and shape. *Arch. Biochem. Biophys.* 313: 47–49.

Sutherland, C., B. S. Renaux, D. J. McKay, and M. P. Walsh. 1994. Phosphorylation of caldesmon by smooth-muscle casein kinase II. *J. Muscle Res. Cell Motil.* 15:440–456.

Szpacenko, A., and R. Dąbrowska. 1986. Functional domain of caldesmon. *FEBS Lett.* 202:182–186.

Velaz, L., R. H. Ingraham, and J. M. Chalovich. 1990. Dissociation of the effect of caldesmon on the ATPase activity and on the binding of smooth heavy meromyosin to actin by partial digestion of caldesmon. *J. Biol. Chem.* 265:2929–2934.

Vibert, P., R. Craig, and W. Lehman. 1993. Three-dimensional reconstruction of caldesmon containing smooth muscle thin filaments. *J. Cell Biol.* 123:313–321.

Vorotnikov, A. V., N. B. Gusiev, S. Hua, J. H. Collins, C. S. Redwood, and S. B. Marston. 1994. Phosphorylation of aorta caldesmon by endogeneous proteolytic fragments of protein kinase C. *J. Muscle Res. Cell Motil.* 15:37–48.

Walsh, M. P. 1991. Calcium-dependent mechanism of regulation of smooth muscle contraction. *Biochem. Cell Biol.* 69:771–800.

Wang, C.-L. A., J. M. Chalovich, P. Graceffa, R. C. Lu, K. Mabuchi, and W. F. Stafford. 1991a. A long helix from the central region of smooth muscle caldesmon. *J. Biol. Chem.* 266:13958–13963.

Wang, C.-L. A., L.-W. C. Wang, S. Xu, R. C. Lu, V. Saavedra-Alanis, and J. Bryan. 1991b. Localization of the calmodulin- and the actin-binding sites of caldesmon. *J Biol. Chem.* 266:9166–9172.